J Atmos Chem
DOI 10.1007/s10874-016-9336-6

Photochemical activation of chlorine by iron-oxide aerosol

Julian Wittmer[1] · **Cornelius Zetzsch**[1,2]

Received: 1 October 2015 / Accepted: 31 March 2016

Abstract The photochemical activation of chlorine by dissolved iron in artificial sea-salt aerosol droplets and by highly dispersed iron oxide (Fe_2O_3) aerosol particles (mainly hematite, specific surface ~150 $m^2\ g^{-1}$) exposed to gaseous HCl, was investigated in humidified air in a Teflon simulation chamber. Employing the radical-clock technique, we quantified the production of gaseous atomic chlorine (Cl) from the irradiated aerosol. When the salt aerosol contained Fe_2O_3 at pH 6, no significant Cl production was observed, even if the dissolution of iron was forced by "weathering" (repeatedly freezing and thawing for five times). Adjusting the pH in the stock suspension to 2.6, 2.2, and 1.9 and equilibrating for one week resulted in a quantifiable amount of dissolved iron (0.03, 0.2, and 0.6 mmol L^{-1}, respectively) and in gaseous Cl production rates of ~1.6, 6, and 8×10^{21} atoms $cm^{-2}\ h^{-1}$, respectively. In a further series of experiments, the pure Fe_2O_3 aerosol was exposed to various levels of gaseous hydrogen chloride (HCl). The resulting Cl production rates ranged from 8×10^{20} Cl atoms $cm^{-2}\ h^{-1}$ (at ~4 ppb HCl) to 5×10^{22} Cl atoms $cm^{-2}\ h^{-1}$ (at ~350 ppb HCl) and confirmed the uptake and conversion of HCl to atomic Cl (at HCl to Cl conversion yields of 2–5 %, depending on the relative humidity). The Fe_2O_3 experiments indicate that iron-induced Cl formation may be important for highly soluble combustion-aerosol particles in marine environments in the presence of gaseous HCl.

Keywords Fe_2O_3 aerosol · Iron oxide · Sea-salt aerosol · Cl activation · HCl uptake

✉ Julian Wittmer
Julian.Wittmer@uni-bayreuth.de

✉ Cornelius Zetzsch
cornelius.zetzsch@mpic.de

[1] Atmospheric Chemistry Research Unit, BayCEER, University of Bayreuth, Dr. Hans-Frisch Straße 1-3, 95448 Bayreuth, Germany

[2] Max Planck Institute for Chemistry, Hahn-Meitner-Weg 1, 55128 Mainz, Germany

Published online: 14 April 2016

1 Introduction

Iron is an essential element of the lithosphere, hydrosphere and biosphere, which is demonstrated by its manifold chemistry having significant implications on the atmosphere. As a bioelement, it mediates metabolic processes and thus indirectly affects the atmospheric carbon footprint. In the atmosphere, iron is mainly present in aerosol particles in form of solid oxides arising naturally basically from arid continental regions (~95 %) or from anthropogenic combustion processes (~5 %; Luo et al. 2008). Volcanic eruptions may significantly contribute to the iron budget in some periods (Duggen et al. 2007). Mineral aerosol particles influence the absorption and reflection of solar radiation, cloud condensation and the gas-phase chemistry. Concerning the latter, in particular the (aqueous) surface chemistry is decisive. The dissolution of ferric oxides in the aqueous phase (e.g. atmospheric waters or quasi-liquid aerosol layer) is driven by salinity, pH, organic (e.g. humic like substances; Al-Abadleh 2015) and inorganic (e.g. chloride; Liu and Millero 2002) or ligands and induces Fenton-like processes that lead to aqueous-phase radicals when exposed to sunlight. Lim et al. (2006), Wittmer et al. (2015a) and Wittmer et al. (2015b) demonstrated that such a system leads to gaseous halogen formation in the presence of halides. The halogen formation is initiated by the photolytic reduction of Fe^{III}-chloride complexes (Miller et al. 1995; Nadtochenko and Kiwi 1998).

The global average iron solubility in aerosol-particle suspensions is estimated to ~1–2 % (Jickells and Spokes 2001), whereas measurements and estimates of the fraction of soluble iron in marine aerosol range from 0 − 95 % depending on the origin of the iron-containing aerosol (e.g. combustion or mineral dust; Schroth et al. 2009), the aerosol pH (Keene et al. 1998), age, size and composition (Zhu et al. 1993; Siefert et al. 1998; Baker et al. 2006; Baker and Croot 2010; Sholkovitz et al. 2012). Atmospheric processing can considerably influence the iron solubility (Mahowald et al. 2009). Rubasinghege et al. (2010) demonstrated the significant role of size and anions in the dissolution of FeOOH. In this context, the interaction between iron-containing particles and gaseous HCl is still relatively unexplored. Zhang and Iwasaka (2001) investigated the Cl deposition on dust particles in a marine atmosphere. Moreover, Sullivan et al. (2007b) determined a Cl mass fraction of 4–9 % in dust particles during a major dust storm and ascribed the enrichment in Cl to the heterogeneous HCl uptake. The behavior of HCl remains unclear when a large fraction of iron oxide is involved in the aerosol (e.g. combustion aerosol particles). The potential uptake may lead to a photochemical activation of chloride, similar to halide media doped with Fe^{III} (Wittmer et al. 2015a, b). The mean natural gaseous HCl concentration in the boundary layer is ~200 ppt (Graedel and Keene 1996) with an annual HCl production rate of 7.6 Tg yr^{-1} (Erickson et al. 1999). Main sources are the dechlorination (e.g. by acid displacement in sea salt), volcanoes, and anthropogenic activities (e.g. coal combustion or biomass burning). The main sink is the heterogeneous deposition on surfaces (Keene et al. 1999). The chemical reaction (mainly with OH) and subsequent Cl production is not an efficient net sink based on the further reactions of Cl with hydrocarbons via H abstraction and thus a regeneration of HCl.

Behnke and Zetzsch (1990) already determined an enhanced production of atomic Cl from HCl uptake at high ozone (O_3) concentrations and relative humidities in the presence of SiO_2 and Fe_2O_3 aerosol particles. Here, we take up the topic of the atmospheric impact of iron oxides exposed to halide media. In particular, we investigated the iron-induced Cl activation from Fe_2O_3-containing sea-salt aerosol particles or from pure iron-oxide aerosol in the presence of HCl. In the latter case, we explored the uptake of gaseous HCl and its

heterogeneous conversion into Cl. The study simulated conditions where Fe_2O_3-containing sea-salt aerosol or pure iron-oxide aerosol are exposed to sunlight in remote marine environments at low trace gas concentrations.

2 Experimental

The experimental set-up was equal to the set-up in Wittmer et al. (2015b). All experiments were conducted at 20 °C in a Teflon smog chamber (Fluorinated Ethylene Propylene - FEP 200A, DuPont, Wilmington, DE, USA) with a volume of ~3.5 m^3 that is continuously flushed with hydrocarbon-free, humidified (temperature-controlled three-neck bottle filled with deionized water (Seralpur pro 90 cn, <0.055 μS cm^{-1})) zero air (zero-air-generator, cmc instruments, <1 ppb O_3, <0.5 ppb NO_X, <100 ppb CH_4) to replenish the air consumption of the connected analyzers (EcoPhysics, CLD 88p coupled with a photolytic converter, PLC 860 for NO and NO_X, and UPK 8001 for O_3) and to maintain a slight overpressure (0.3 − 1 Pa). The chamber is suspended above a solar simulator, providing an actinic flux comparable to the tropospheric sunlight on the 50th latitude in the tropospheric summer. More detailed specifications can be found elsewhere (Buxmann et al. 2012; Bleicher et al. 2014; Wittmer et al. 2015a). After every experiment, the chamber was either cleaned by deionized water or the whole Teflon film was exchanged. In both cases, the chamber was (re-)conditioned by irradiation with four UV lamps (Phillips TUV 55 W, λ = 253.7 nm) in the presence of >1 ppm O_3 at high RH.

In principle, two types of experiments were performed. The first series of experiments consisted of nebulizing (Ultrasonic nebulizer: Quick Ohm QUV-HEV FT25/16-A, 35 W, 1.63 MHz) and irradiating an artificial sea-salt stock solution (containing 824 mg L^{-1} NaCl, 314 mg L^{-1} $Na_2SO_4 \times 10\ H_2O$, 176 mg L^{-1} $MgCl_2$, 52 mg L^{-1} $CaCl_2 \times 2\ H_2O$, 24 mg L^{-1} KCl, 6.9 mg L^{-1} $NaHCO_3$, 3.4 mg L^{-1} KBr, 0.9 mg L^{-1} H_3BO_3, and 0.1 mg L^{-1} NaF; Kester et al. 1967) doped with Fe_2O_3 (Sicotrans Orange L2515D, BASF) with a specific surface area: 152 $m^2\ g^{-1}$ (according to a BET measurement at the Faculty of Engineering Sciences, University of Bayreuth). The Mössbauer analysis of Sicotrans Orange (evaluated by the Bavarian Research Institute of Experimental Geochemistry and Geophysics at Bayreuth using the program MossA; Prescher et al. 2012) revealed the dominant presence of Fe^{3+} in the form of α-Fe_2O_3 (hematite), a phase containing paramagnetic Fe^{3+} and a fraction of Fe^{2+} and/or Fe^{3+} showing slow paramagnetic relaxation (Fig. 1).

In addition to an untreated run, the dissolution of Fe_2O_3 in the sea salt was promoted by acidification or repeated freezing/thawing processes. For each experiment, 17 mg of Fe_2O_3 were stirred into 100 mL of the artificial seawater solution to obtain a molar ratio of ~0.08 between solid (and dissolved) iron and Cl^-. This contribution is comparable to the largest Fe^{III} concentration in Wittmer et al. (2015b) where $FeCl_3$ was dissolved in artificial seawater. The powder formed a suspension with Fe_2O_3 grains sinking to the bottom within 3–5 min. Therefore, the flask was shaken before filling ~50 ml into the nebulizer. For some samples, the pH was reduced to 2.6, 2.2 and 1.9 (measured by a pH meter, pH 3110, WTW) by adding 30, 55 and 110 μL of HCl (Sigma–Aldrich ACS, 37 %), respectively. In this way, the Cl^- concentration in the stock solution increased from 28 to 31.6, 34.6 and 41 mmol L^{-1}. After 16 h, 113 h and 186 h, an aliquot of each sample was passed through a 0.025 μm filter (Whatman Anotop 10 Plus) combined with a 0.45 μm pre-filter (Millipore), to determine the

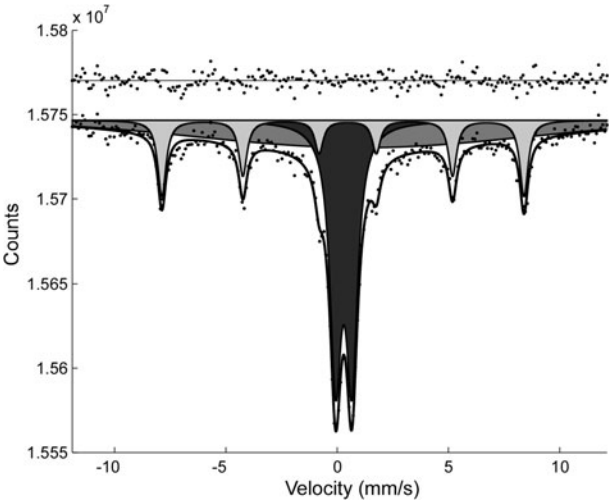

Fig. 1 Room temperature Mössbauer spectrum of Sicotrans Orange L 2515. The spectrum is fitted to a magnetic sextet assigned to α-Fe_2O_3 (light grey, 19 %), a quadrupole doublet assigned to Fe^{3+} (*dark grey*, 39 %) and a broad absorption assigned to Fe^{2+} and/or Fe^{3+} (*medium grey*, 42 %). The relative areas of the different components indicate roughly the relative abundance of the different iron species. The residual (difference between the fitted curve and experimental data) is shown above the spectrum and the velocity scale is relative to α-Fe_2O_3. The spectrum was collected for 13 days and was evaluated by Dr. Catherine McCammon (BGI Bayreuth, Germany) using the program MossA (Prescher et al. 2012)

amount of dissolved iron (Fe_d) by ICP-OES (Central Analytics, BayCEER, University of Bayreuth). The obtained filtrated solution may contain smaller iron colloids (<0.025 μm) that would also be detected by ICP-OES and may distort the given Fe_d concentrations. However, the amount of iron from colloids is rather negligible with regard to the sample without pH adjustment, where the remaining colloids did not lead to a detectable amount of iron (detection limit ~0.001 mmol L^{-1}).

In a second series of experiments, hydrated Fe_2O_3 or SiO_2 aerosol particles were generated by nebulizing a suspension of the Sicotrans Orange powder or Aerosil 200 (Evonik Industries, specific surface of 200 m^2 g^{-1}) in water. The resulting aerosol particles were exposed to various levels of gaseous (evaporated) HCl by injecting known amounts of concentrated hydrochloric acid (Sigma-Aldrich, ACS, 37 %).

The aerosol was produced in accordance to Wittmer et al. (2015b), with the only difference that pure nitrogen was applied for injection to avoid the sonochemical formation of nitrate and nitrite (Supeno and Kruus 2000). The aerosol size distributions and concentrations were monitored by an electrostatic classifier (TSI, 3071) in combination with a bipolar neutralizer (^{85}Kr) and a condensation nucleus counter (TSI, 3020). Scanning and data evaluation were performed by a custom written software (Balzer 2012). Typical resulting size distributions, obtained after 30–60 min of injection, are shown in Fig. 2. Based on these distributions (measured every 15 min), the aerosol surface is calculated. For some distributions, a slightly bi- or trimodal shape is recognizable probably caused by the laminar and turbulent coagulation during the nebulization process at high temperatures and number densities within the nebulizer (Wang et al. 2008). For the suspensions of Aerosil 200 and Sicotrans Orange in deionized water, we observed a less effective ultrasonic aerosol production indicated by much lower aerosol loads at comparable injection times to the artificial seawater experiments. The

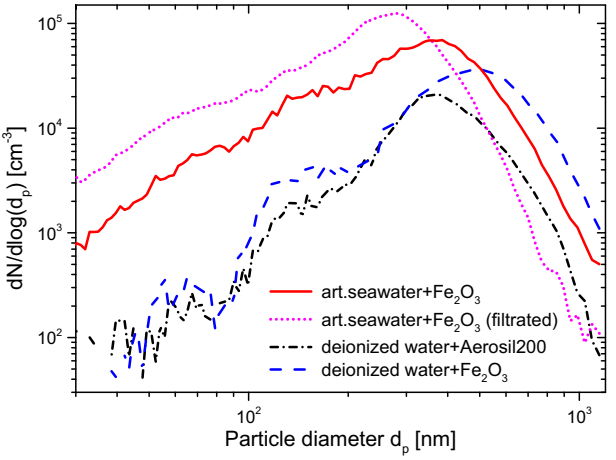

Fig. 2 Initial (multiple-charge corrected) size distributions for aerosol particles generated by the ultrasonic nebulizer (30–60 min injection time) from the stock solutions (filtrated and unfiltered artificial seawater, doped with Fe_2O_3, Aerosil 200 in deionized water, and Fe_2O_3 in deionized water)

determined surface lifetimes were $\tau_s = 4510 \pm 952$ s for the pure Fe_2O_3 aerosol and $\tau_s \sim 4800 \pm 800$ s for the Fe_2O_3 + artificial seawater aerosol. Note that the specific surface of the aerosol particles is much larger due to the formation of porous agglomerates.

The production rates and total production of Cl and OH radicals were determined by the radical clock method (Behnke et al. 1988; Zetzsch and Behnke 1993), monitoring the degradation pattern of selected hydrocarbons (2,2-dimethylpropane, Linde, ≥ 99 %; 2,2-dimethylbutane, Aldrich, ≥ 99 %; 2,2,4-trimethylpentane, Janssen ≥ 99 %; toluene, Aldrich ≥ 99.9 %) by a gas chromatograph with flame ionization detector (Siemens Sichromat 2) with a capillary column (Al_2O_3-PLOT) equipped with a custom-built liquid nitrogen cooled cryo-trap enrichment (sampling flow 100 mL min^{-1} dried by a Nafion dryer). The combined time profiles of the hydrocarbons allow us to quantify the quasistationary radical concentrations based on the individual rate constants ($k_{Cl,i}$; $k_{OH,i}$) of the hydrocarbons (HC_i) towards Cl and OH.

$$-\frac{\mathrm{dln}[\mathrm{HC}_i]}{\mathrm{d}t} = \mathrm{k}_{\mathrm{Cl},i}[\mathrm{Cl}] + \mathrm{k}_{\mathrm{OH},i}[\mathrm{OH}] \tag{1}$$

These quasistationary concentrations of the radicals were corrected for the reactivity of the system according to Wittmer et al. (2015a) leading to a minimum (considering the actual, measured hydrocarbon concentrations) and maximum (assuming a reactivity of the degradation products comparable to the initial reactivity of the system) total production Q_{Cl} and production rate dQ_{Cl}/dt.

$$\frac{\mathrm{d}Q_{\mathrm{Cl}}}{\mathrm{d}t} = \sum_i \mathrm{k}_{\mathrm{Cl},i}[\mathrm{HC}_i]_t[\mathrm{Cl}]_t \tag{2}$$

Q_{Cl} and dQ_{Cl}/dt are corrected for the chamber volume and normalized by the effective active aerosol surface A_{eff}, considering the actual measured aerosol surface and the active, deposited surface that forms due to the deposition on the Teflon walls.

$$\frac{\mathrm{d}Q_{\mathrm{abs}}}{\mathrm{d}t} = \frac{\frac{\mathrm{d}Q_{\mathrm{Cl}}}{\mathrm{d}t} \times \mathrm{V}_{\mathrm{Ch}}}{A_{\mathrm{eff}}(t)} \tag{3}$$

The detailed calculation of A_{eff} is described in Wittmer et al. (2015b). The result is the (minimum and maximum) total production (rate) Q_{abs} (dQ_{abs}/dt) of Cl radicals per square centimeter of aerosol surface.

3 Results and discussion

3.1 Cl production from Fe_2O_3 in artificial sea-salt aerosol

Figure 3 displays the measured iron concentrations as a function of time for each sample. As already explored in precipitation studies, the equilibration takes at least 7 days to stoichiometry (Kuma et al. 1996; Liu and Millero 2002). The dissolution proceeds via

$$Fe_2O_3 + 6H^+ \leftrightarrow 2Fe^{3+} + 3H_2O \quad (R1)$$

and depends on the further stepwise formation of Fe^{III}-hydroxy and Fe^{III}-chloride complexes (Liu and Millero 2002; Wittmer et al. 2015a), explaining the strong increase of dissolved iron with pH (Fig. 3). For instance, Nadtochenko and Kiwi (1998) and Wittmer et al. (2015b) identified $FeCl^{2+}$ and $FeCl_2^+$ (R6, R7, Table 1) as the key complexes (coordinated water molecules omitted) that are dominant in the acidic pH range (<4.5) at high salinity and form Cl radicals in the aqueous phase that combine and lead to degassing of Cl_2. At higher pH, $FeOH^{2+}$ and $Fe(OH)_2^+$ (R2, R3, Table 1) become relevant as a source of OH radicals (classical photo-Fenton) but can also form Cl_2 in the presence of Cl^-. For a more detailed discussion of the speciation parameters and the kinetic mechanism of the Cl_2 production, we refer to Wittmer et al. (2015b). The sea-salt matrix promotes the dissolution of iron, as indicated by the larger amount of dissolved iron in the sea-salt sample (pH 2.6, 30 μL HCl added) compared to the sample with 17 mg Fe_2O_3 in 100 mL deionized water (pH 2.5, 40 μL HCl added). The dissolution of Fe_2O_3 finally resulted in Fe_d/Cl^- ratios of ~0.001 (pH 2.6), ~0.006 (pH 2.2) and ~0.014 (pH 1.9) in the artificial seawater solutions. The filtrated samples of Fe_2O_3-doped artificial seawater and deionized water without pH adjustment did not contain detectable amounts of iron (<0.0001 mmol L^{-1}). The high sensitivity of Fe_d toward small changes in pH was already explored by Zhu et al. (1992) in detail. For hematite, they found a variation in solubility of 4 orders of magnitude in the pH range from 0.5 to 2.

In the first experiment, the Fe_2O_3 – artificial seawater mixture without pH adjustment was applied. The time profiles of the hydrocarbons did not show a significant depletion, implying a

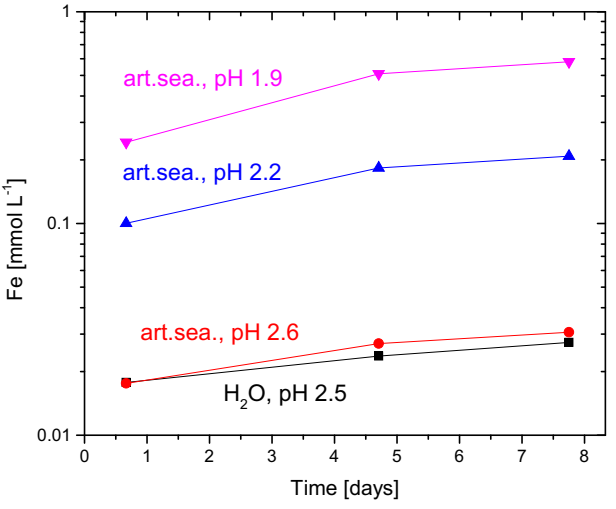

Fig. 3 The concentration of quasi-dissolved iron in artificial seawater and deionized water at various pHs and 25 °C as a function of time. The samples were passed through a 0.025-μm filter (Whatman Anotop 10 Plus) combined with a 0.45 μm pre-filter (Millipore) and the iron content was determined by ICP-OES

Table 1 Relevant equilibria influencing the speciation of iron complexes in a saline solution

$Fe^{3+} + H_2O \leftrightarrow FeOH^{2+} + H^+$	(R2)
$Fe^{3+} + 2H_2O \leftrightarrow Fe(OH)_2^{+} + 2H^+$	(R3)
$Fe^{3+} + 3H_2O \leftrightarrow Fe(OH)_3 + 3H^+$	(R4)
$Fe^{3+} + 4H_2O \leftrightarrow Fe(OH)_4^{-} + 4H^+$	(R5)
$Fe^{3+} + Cl^- \leftrightarrow FeCl^{2+}$	(R6)
$Fe^{3+} + 2Cl^- \leftrightarrow FeCl_2^{+}$	(R7)
$Fe^{3+} + 3Cl^- \leftrightarrow FeCl_3$	(R8)

Cl production rate below the detection limit ($<5 \times 10^{17}$ atoms cm^{-2} s^{-1}). One main reason is the low fraction of dissolved Fe_2O_3, as indicated by the pH of 6 and by an iron concentration of the filtrated aliquot below the detection limit (Table 2). E.g. Byrne and Kester (1976), Kuma et al. (1996) and Liu and Millero (2002) determined a very low amount of dissolved Fe^{III} from Fe^{III}-hydroxides in seawater at this pH range (e.g. 5.53×10^{-14} mol kg^{-1} for Fe_2O_3 in seawater at pH 5 (Zhu et al. 1992) or $\log[Fe^{III}] = -6.8$ at pH 5 for ferric hydroxide (Liu and Millero 2002). Even if the pH and the ionic strength change after nebulization, the time to reach the dissolution equilibrium during the experiment (typically 3 h) is quite short. Therefore, the high ionic strength in the produced aerosol has a negligible effect in this short timescale compared to the pH of the stock solution. Concerning the change of ion concentrations from the initial solution to the aerosol phase, one may assume a saturated salt solution (~6.1 mol Cl^- L^{-1}) after a rapid equilibration of the liquid aerosol phase with its surrounding.

To alternatively accelerate and promote the dissolution of the iron oxide, an aliquot of the Sicotrans-artificial seawater mixture was frozen at −20 °C for 1–3 h and thawed again at 20 °C for five times. Jeong et al. (2012) determined a greatly enhanced dissolution due to this process at acidic pH conditions (pH 2–4) in the dark. However, we did not observe an effect related to the Fe^{III} − induced Cl production. The impact of the accelerated dissolution was below the detection limit. Based on the significant detection starting from a molar $Fe^{III}/Cl^- > 0.001$

Table 2 Overview on pH and molar Fe_d/Cl^- ratio (Fe_d = total amount of dissolved iron) of the nebulized artificial seawater (100 ml) + Fe_2O_3 (17 mg) suspensions, total initial reactivities of the injected hydrocarbons towards Cl and OH, initial active aerosol surface at the beginning of irradiation, resulting quasistationary Cl_{qs} and OH_{qs} concentrations during the first hour and the resulting total Cl production per cm^{-2} aerosol surface during the first hour

pH	Molar Fe_d/Cl^- ratio	Fe_d (mmol L^{-1})[c]	Initial reactivity (s^{-1})		Initial A_{eff} ($10^{-3} \cdot m^2$ m^{-3})	X_{qs} (10^5 / 10^6 atoms cm^{-3})[d]		$Q_{Cl_{abs}}$ (10^{21} atoms cm^{-2} h^{-1})
			Cl	OH		Cl	OH	
6	$<3 \times 10^{-5}$	<0.001[e]	86	1.5	42.1	< 0.1[e]	10	< 1[e]
6[a]	$<3 \times 10^{-5}$	<0.001[e]	101	2.1	49	< 0.1[e]	3	< 1[e]
2.6	0.001	0.031	118	2.3	19.3	1.8	2.6	1.6–1.7
2.6[b]	0.001	0.031	110	2.6	12.8	4.7	5.6	5.6–6.8
2.2	0.006	0.21	106	2.5	14.3	5.5	2.4	5.6–6.6
1.9	0.014	0.58	100	2.5	16.8	10	n.d.[f]	7.0–9.3

[a] Five times frozen and thawed, [b] Filtrated, [c] after 7 days of equilibration, [d] mean steady state concentrations during the 1st hour, [e] below the detection limit, [f] below the detection limit because of too high Cl concentration

(see Table 2), we conclude that at least ~1 % of the added Fe_2O_3 has to be dissolved in artificial seawater to detect a gaseous Cl production. Although, accelerating the iron-oxide dissolution rates more than 2 times by freezing (Jeong et al. 2012), the dissolved fraction remains far below 1 %, justified by the very low solubility value of $\log[Fe^{III}] = -11.0$ for artificial seawater at 25 °C and pH = 8.1 (Liu and Millero 2002).

In contrast to the samples without pH adjustment, the nebulization and irradiation of the pH adjusted samples resulted in a significant Cl production. Figure 4 shows the Cl production and the Fe_d/Cl^- ratio in the nebulized solution as a function of the pH. The Cl source clearly increases with increasing acidity and thus with the amount of dissolved iron and the increasing Fe/Cl^-. At the highest pH of 2.6 in this series ($Fe/Cl^- = 0.001$), we observed a Cl production of $(1.6-1.7)\times10^{21}$ atoms cm^{-2} h^{-1}, at pH 2.2 ($Fe/Cl^- = 0.006$) the Cl production was $(5.6-6.6)\times10^{21}$ atoms cm^{-2} h^{-1}, and it was $(7.0-9.3)\times10^{21}$ Cl atoms cm^{-2} h^{-1} at the lowest pH of 1.9 ($Fe/Cl^- = 0.014$). The increase shows a non-linear relation with pH (or amount of dissolved iron), that is discussed in the following.

The fraction of active iron (λ_{Fe}) was calculated according to Wittmer et al. (2015b), resulting in 2010 % for pH 2.6, 1220 % for pH 2.2, and 620 % for pH 1.9. These high iron activities of more than 100 % indicate a multiple recycling process of the dissolved iron or even a further dissolution of Fe_2O_3 in the quasi-liquid layer of the aerosol. The contribution of additional Cl activation mechanisms due to zero air impurities (e.g. O_3 and NO_X) is supposed to be small when comparing the values to the relatively low λ_{Fe} of 50–150 % obtained in Wittmer et al. (2015b) for iron-doped artificial sea-salt aerosol exposed to O_3 and NO_X. Furthermore, the decrease of λ_{Fe} with lower pH demonstrates the non-linear relation of pH and Cl production (the ratio between produced Cl and Fe_d decreases with lowering the pH but should be constant in a linear relation). This is in contrast to the results in Wittmer et al. (2015b), where λ_{Fe} increases when decreasing the pH from 4 to 2.2. The discussed samples in the present study are in the pH range from 1.5 to 3, where the fractions of the Fe^{III}-Cl complexes are stable. However, the fractions of Fe^{III}-hydroxy complexes ($FeOH^{2+}$, $Fe(OH)_2^+$) decrease significantly with increasing acidity (Wittmer et al. 2015b) and the photochemical

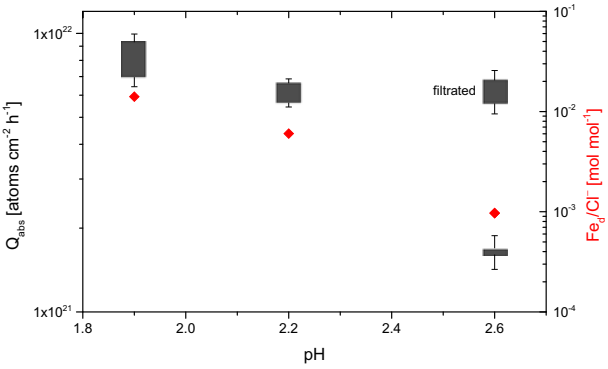

Fig. 4 Total amount of Cl atoms per hour and per cm^2 aerosol surface produced at various pHs (HCl additions) by the nebulized suspensions of Fe_2O_3 in artificial seawater (*black bars*, left ordinate) and the corresponding Fe_d/Cl^- ratios determined for the filtrated aliquots (*red diamonds*, right ordinate). In each experiment, the Fe_2O_3-artificial seawater suspension was nebulized except for the labeled experiment where a filtrated solution was applied. The lower and upper margins of the *bars* represent the minimal and maximal values. The *error bars* represent the respective negative minimum and the positive maximum uncertainty

formation of $OH^{\cdot}$ radicals and H_2O_2 (R9), and thus the re-oxidation of Fe^{II} to Fe^{III} (R10), become inefficient (λ_{Fe} decreases).

$$OH^{\cdot} + OH^{\cdot} \rightarrow H_2O_2 \quad \text{(R9)}$$

$$Fe^{2+} + H_2O_2 \rightarrow Fe^{3+} + OH^{\cdot} + OH^{-} \quad \text{(R10)}$$

Indeed, the highly concentrated Cl^- anion scavenges $OH^{\cdot}$ to form $Cl_2^{\cdot -}$ and potentially degassing Cl_2 (R11–R14) but inhibits the catalyzing effect of iron in case of low $OH^{\cdot}$ concentrations (R9, R10, R15, Kiwi et al. 2000; Machulek et al. 2006).

$$OH^{\cdot} + Cl^{-} \rightarrow ClOH^{\cdot} \quad \text{(R11)}$$

$$ClOH^{\cdot} + H^{+} \rightarrow Cl^{\cdot} + H_2O \quad \text{(R12)}$$

$$Cl^{\cdot} + Cl^{-} \rightarrow Cl_2^{\cdot -} \quad \text{(R13)}$$

$$Cl_2^{\cdot -} + Cl^{-} \rightarrow Cl_2 \quad \text{(R14)}$$

$$Fe^{2+} + OH^{\cdot} \rightarrow Fe^{3+} + OH^{-} \quad \text{(R15)}$$

Moreover, Machulek et al. (2007) related the decreasing efficiency of the Fenton process from pH 3 to 1 to the reduction of Fe^{III} by H_2O_2 (R16) that depends on acidity, and to the dominant formation of the less reactive $Cl_2^{\cdot -}$ radical (and not $OH^{\cdot}$). The potential formation of oxoiron (IV) (FeO^{2+}) at this pH range may also influence the $OH^{\cdot}$ formation (Pignatello et al. 1999).

$$Fe^{3+} + H_2O_2 \leftrightarrow Fe^{2+} + HO_2^{\cdot} + H^{+} \quad \text{(R16)}$$

To investigate possible matrix and dissolution effects in the aerosol phase, a filtrated aliquot of the pH 2.6 sample was nebulized and irradiated in order to compare the results to the run including solid Fe_2O_3. The comparison led to a 3.5–4 times higher Cl production of the filtrated experiment ($5.6-6.8\times10^{21}$ Cl atoms cm^{-2} h^{-1}). The strong increase may originate from the larger specific aerosol surface based on the smaller most abundant particle diameter for the filtrated sample (surface to volume ratio: 1.79×10^{7} m^{-1}) compared to the unfiltrated sample (surface to volume ratio: 1.50×10^{7} m^{-1}), as illustrated in Fig. 2. The higher surface to volume ratio may cause an enhanced availability of iron, indicated by the high λ_{Fe} of 7840 %.

3.2 Cl production from HCl uptake on Fe_2O_3

We explored the heterogeneous Cl production from Fe_2O_3 aerosol particles by the uptake of HCl in a series of experiments. It should be noted that the given HCl concentrations may contain an uncertainty of 50 % based on the adsorption on the FEP-Teflon walls (Zetzsch and Behnke 1993), but due to the same conditions for every experiment, a relative comparison is

still significant. An aerosol-free experiment resulted in a production of $(2.6-2.7)\times10^{10}$ Cl atoms cm^{-3} h^{-1} (~7.4×10^{6} Cl atoms cm^{-3} s^{-1}) at a quasistationary OH concentration of ~2×10^{6} cm^{-3}. The theoretical Cl production rate at 345 ppb HCl and 2×10^{6} cm^{-3} OH is 1.28×10^{7} cm^{-3} s^{-1} ($k_{HCl+OH}=7.6\times10^{-13}$ cm^{3} $molecules^{-1}$ s^{-1} at 20 °C, Atkinson et al. 2007), based on the homogeneous gas-phase reaction

$$HCl_{(g)} + OH \rightarrow Cl + H_2O \quad (R17)$$

Assuming that Cl is formed only homogeneously in this experiment implies a reproducibility (ρ) of 56–59 %, comparing the amount of HCl retrieved from the measured Cl production and the injected amount of HCl. The measured lower value is probably caused by injection and adsorption losses of HCl (and thus lower gaseous HCl concentrations than calculated).

To distinguish the iron-induced, heterogeneous Cl formation from the fraction of Cl formed by the reaction of gaseous HCl with OH and by non-iron induced, heterogeneous Cl formation, several blank runs were conducted. The relevant OH concentrations in these experiments originate from trace impurities of NO_X (Wittmer et al. 2015a) and from photolysis of HONO degassing from the Teflon film (background OH production rate in dry zero air ~10^{7} molecules cm^{-3} s^{-1}, Bartolomei et al. 2015). As might be expected, the injection and irradiation of pure iron-oxide aerosol resulted in Cl concentrations below the detection limit, since no chlorine is present in the system to be activated. Further experiments included the injection and irradiation of 5 μL HCl (~ 345 ppb gas phase mixing ratio in the smog chamber) in the presence of non-catalytic, UV transparent SiO_2 aerosol particles (Aerosil 200) at 40–50 % RH.

The addition of SiO_2 left the OH concentrations unaffected but enhanced the formation of Cl atoms to $(1.1-1.2)\times10^{11}$ Cl atoms cm^{-3} h^{-1} (related to the aerosol surface: $2.6-2.7\times10^{21}$ Cl atoms cm^{-2} h^{-1}) compared to the aerosol-free blank experiment. The approximately four times higher Cl production is caused by the increase of hydrophilic surface available for heterogeneous reaction (according to the experience of Zetzsch and Behnke 1993, with Aerosil 200 and Sicotrans orange in FEP-Teflon bags in comparison with blank runs). Although the additional aerosol surface of 0.018 m^{2} m^{-3} is quite low compared to the wall surface (3.8 m^{2} m^{-3}), the surrounding aqueous layer of the aerosol (due to the nebulization of a suspension) absorbs gaseous HCl, enabling the dissociated Cl^{-} anions to be converted to gaseous Cl radicals by the known activation processes (e.g. Rossi 2003). Once highly soluble $HOCl_{(g)}$ is formed via O_3 (from the NO_X impurities) and HO_2 (from the degradation of hydrocarbons), it rapidly leads to degassing of photolabile Cl_2 ($J_{Cl2}=1.55\times10^{-3}$ s^{-1}), particularly on an acidic surface containing Cl^{-} in the absence of Br^{-} (e.g. Vogt et al. 1996):

$$HOCl_{(g)} + Cl^{-}_{(aq)} \rightarrow Cl_{2(g)} + OH^{-}_{(aq)} \quad (R18)$$

Moreover, the uptake of OH and subsequent reaction with $Cl^{-}_{(aq)}$ may also contribute to this process (Knipping et al. 2000). As already mentioned above, a heterogeneous Cl production from HCl was also reported by Zetzsch and Behnke (1993), who measured an eight times higher maximum Cl formation in the presence of SiO_2 aerosol particles as compared to the blank run.

When Fe_2O_3 aerosol particles and 5 μL HCl were added, the Cl production was significantly enhanced to $(2.6-3.0)\times10^{11}$ Cl atoms cm^{-3} h^{-1} (related to the aerosol surface: $5.7-6.6\times10^{22}$ Cl atoms cm^{-2} h^{-1}) at a mean OH concentration of ~5×10^{6} cm^{-3}. The higher

quasistationary OH concentration in the Fe_2O_3 experiment at comparable hydrocarbon reactivities were caused by the slightly higher RH (~60 %), but also by an enhanced HC oxidation by Cl and subsequent HO_2 and OH formation. Zetzsch (1987) and Behnke and Zetzsch (1988) detected elevated OH concentrations in the presence of Fe_2O_3 aerosol (containing Cl^-, SO_4^{2-}, and NO_3^-) and O_3 as well. As indicated by the depletion of 29 ppb of hydrocarbons by the reaction with Cl during the first 150 min, the contribution of HCl formed by the depletion of hydrocarbons remains below 10 % (assuming no further reactivity of the reaction products). This also applies to the other experiments with varying HCl concentrations (Table 3).

The iron-free blank experiments represent a background value for the HCl conversion by OH and additional heterogeneous processes. To better compare the background formation with the iron induced Cl formation, the measured Cl production in the SiO_2 experiment is subtracted by the result in the aerosol-free experiment and normalized by the aerosol surface to obtain a heterogeneous and homogeneous background production. Thus, a heterogeneous contribution of 3–3.5 % ($Q_{bg,het} = 2.0 - 2.1 \times 10^{21}$ Cl atoms cm^{-2} h^{-1}) and a homogeneous contribution of ~9–10 % ($Q_{bg,hom} = 2.6 - 2.7 \times 10^{10}$ Cl atoms cm^{-3} h^{-1}) to the iron-induced Cl production was estimated for the experiments applying 5 μL HCl (Fig. 5). The homogeneous contribution may rise with increasing OH concentrations at similar hydrocarbon reactivities and HCl concentrations. Assuming a proportional increase of $Q_{bg,hom}$ with increasing OH concentrations means a maximum effective homogeneous fraction of ~23–25 % of produced Cl in the Fe_2O_3 experiment (comparing the OH concentration of 2×10^6 cm^{-3} in the aerosol-free experiment with 5×10^6 cm^{-3} in the 5 μL HCl experiment). However, this number represents an upper limit of homogeneous contribution based on the assumption of a constant

Table 3 Overview on the experiments with nebulized deionized water (200 ml) + Fe_2O_3 (0.5 g) or SiO_2 suspensions and varying HCl injections

Injected HCl [μL] / HCl mixing ratio [ppb]	Initial reactivity (s^{-1})		Aerosol material	Initial A_{eff} ($10^{-3} \cdot m^2$ m^{-3})	RH [%]	X_{qs} concentration (10^5 / 10^6 radicals cm^{-3})[a]		$Q_{Cl,abs}$ (10^{21} atoms cm^{-2} h^{-1})	$Q_{Cl,eff}$ (10^{21} atoms cm^{-2} h^{-1})
	Cl	OH				Cl	OH		
5 / 345	164	3.9	blank	0	40	0.5	2	n.d.[c]	n.d.[c]
5 / 345	135	3.1	SiO_2	19	52	2.6	2	2.6–2.7	2.0–2.1
0 / 0	174	4.2	Fe_2O_3	8.0	76	< 0.1[b]	10	< 1[b]	< 1[b]
0.6 / 41	113	2.6	Fe_2O_3	5.6	52	1.2	7.4	3.6–3.8	0.77–0.83
1.2 / 83	119	2.9	Fe_2O_3	4.1	59	1.5	4.6	6.4–6.6	2.8–2.9
2.5 / 173	161	4.1	Fe_2O_3	1.9	76	1.2	6.9	15–16	2.3–2.8
2.5 / 173	147	3.7	Fe_2O_3	1.1	42	4.2	3.3	90–104	78–91
3.5 / 242	128	3.0	Fe_2O_3	4.2	57	4.9	8.5	21–23	13–14
5 / 345	169	4.1	Fe_2O_3	1.5	61	4.9	5	57–66	41–49

Total initial reactivities of the injected hydrocarbons towards Cl and OH, initial active aerosol surface at the beginning of irradiation, relative humidity, resulting quasistationary Cl_{qs} and OH_{qs} concentrations during the first hour, the resulting absolute (Q_{abs}) and corrected (Q_{eff}) total Cl productions per cm^{-2} aerosol surface during the first hour are listed

[a] mean steady state concentrations during the 1st hour, [b] below the detection limit, [c] not evaluable since no aerosol phase present

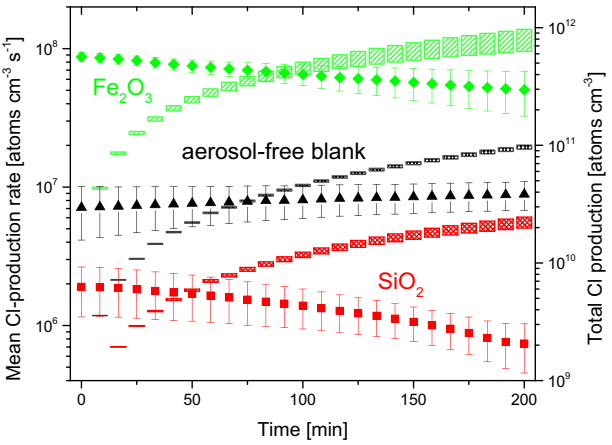

Fig. 5 Mean Cl production rate (*symbols*, left ordinate) and total Cl production (*bars*, right ordinate) of the Fe_2O_3, SiO_2 and aerosol free experiments with 5 μL HCl injected, respectively. For a better comparison of the Fe_2O_3 and the heterogeneous Cl production evaluated in the SiO_2 experiments, the values for SiO_2 were corrected for the homogeneous production and normalized with the ratio of the surface areas (A_{SiO2}/A_{Fe2O3})

HCl concentration with time (justified by the "recycling" of HCl due to hydrocarbon degradation) without injection and adsorption losses.

In the following, the background Cl production is subtracted in order to calculate an effective Cl production Q_{eff} from the determined total production at time t:

$$Q_{\mathrm{eff}}(t) = \frac{(Q_{Cl}(t) - \rho \times [OH] \times [HCl] \times k_{\mathrm{HCl+OH}} \times t) \times V_{\mathrm{Ch}}}{A_{\mathrm{eff}}(t)} - Q_{\mathrm{bg,het}}(t) \qquad (4)$$

where $Q_{\mathrm{Cl}}(t)$ is the integrated total Cl production (atoms cm^{-3}) at time t, [OH] and [HCl] are the quasistationary OH and HCl concentrations (assumed to be constant), V_{Ch} is the chamber volume, A_{eff}(t) is the effective surface area (consisting of the measured aerosol surface and the wall contribution, see Wittmer et al. 2015b), and $Q_{\mathrm{bg,het}}$ the integrated heterogeneous background production at time t. The calculation of Q_{eff} strengthens the comparison of the experiments with various amounts of injected HCl and spares respective blank experiments.

Figure 6 illustrates Q_{eff} for various amounts of HCl injected at a RH of 52–61 %. The lower and upper margins of the bars represent the minimal and maximal values. The error bars

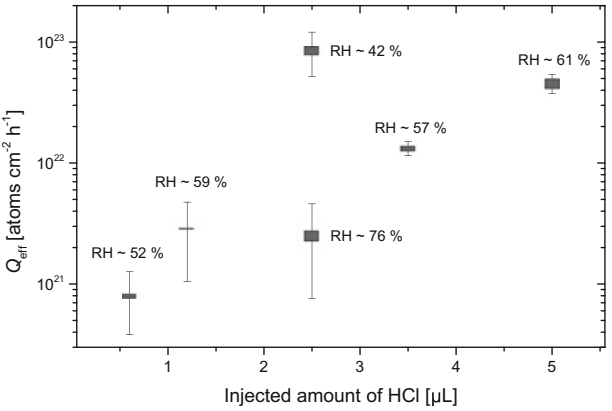

Fig. 6 Total amount of Cl atoms per hour and per cm^2 aerosol surface (corrected for the heterogeneous and homogeneous background) produced at various HCl concentrations. The RH is labeled for each experiment. The lower and upper margins of the *bars* represent the minimal and maximal values. The error *bars* represent the respective negative minimum and the positive maximum uncertainty

represent the respective negative minimum and the positive maximum uncertainty (calculated based on statistical evaluation; Wittmer et al. 2015b). With increasing HCl concentrations an expected increase of Q_{eff} was observed from ~0.8×10^{21} Cl atoms cm^{-2} h^{-1} (for 0.6 μL HCl) to $(41-49) \times 10^{21}$ Cl atoms cm^{-2} h^{-1} (for 5 μL HCl). A not considered influence on the Q_{eff} determination is the wall loss of HCl (by water on the Teflon film or the dry Teflon film). Important hints that the RH affects the gaseous HCl concentration give the experiments with the same amount of HCl injected (2.5 μL) at different RH (42 % and 76 %). The low RH experiment resulted in a significantly higher Cl production ($78-91 \times 10^{21}$ Cl atoms cm^{-2} h^{-1}) compared to the high RH run ($2.3-2.8 \times 10^{21}$ Cl atoms cm^{-2} h^{-1}). Based on the measurements by Svensson et al. (1987) and the formula given by Wahner et al. (1998) the amount of water adsorbed on the Teflon film is ~3.7 mg m^{-2} at 42 % RH (low RH case), ~6 mg m^{-2} at 60 % RH, and ~10 mg m^{-2} at 75 % RH (high RH case). The exponential increase of adsorbed water with increasing RH may intensify the wall sink for HCl and thus explain the strong effect on the Cl production as observed in our experiments. When adsorbed on the "iron-free" Teflon film, HCl contributes to a negligible extent to the halogen activation. E.g. Buxmann et al. (2015) did not find a contribution of deposited HCl and HBr in a comparable system. The number of adsorbed layers on the aerosol particles may dilute the QLM and additionally retarding the activation, even if the layer thickness changes slowly at this RH range (Cwiertny et al. 2008).

In order to estimate the efficiency of the HCl to Cl conversion on the aerosol particles, the fraction of activated chlorine (φ_{Cl}) was calculated by dividing the total (molar) amount of produced Cl atoms Q_{Cl} (including the homogeneous background correction) by the total (molar) amount of injected HCl ($\mathrm{HCl_{inj}}$):

$$\varphi_{\mathrm{Cl}}(t) = \frac{Q_{Cl}(t) - \rho \times [OH] \times [HCl] \times k_{\mathrm{HCl+OH}} \times t}{\mathrm{HCl_{inj}}} \quad (5)$$

The resulting conversion rate during the first hour against the initial aerosol surface is shown in Fig. 7. No clear dependence of φ_{Cl} on the provided aerosol surface was noticed. The various runs show a comparable HCl conversion in the range of 2–5 % except for the value obtained from the high RH experiment (φ_{Cl} below 1 %).

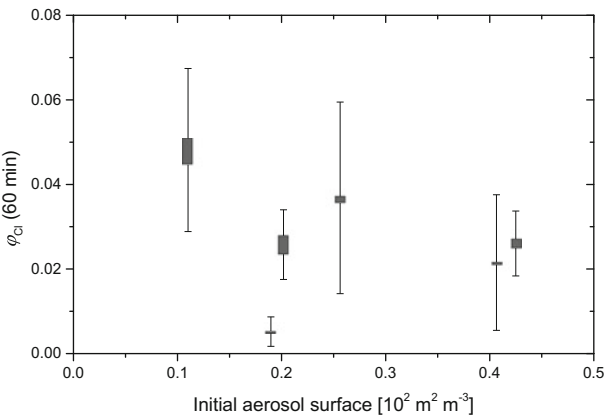

Fig. 7 Conversion rate φ_{Cl} of HCl to Cl within the first hour against the initial aerosol surface for the performed Fe_2O_3 experiments with various amounts of HCl added. The lower and upper margins of the *bars* represent the minimal and maximal values. The *error bars* represent the respective negative minimum and the positive maximum uncertainty

4 Environmental significance

Our results indicate that iron-containing aerosol can become photochemically active during atmospheric processing, especially in marine environments when it comes into contact with sea salt or HCl. The pH of aged sea-salt aerosol is typically in the acidic range from 2 to 4, e.g. depending on the air pollutants and the RH (Keene and Savoie 1998). At this pH, Fe_2O_3 is dissolved in significant amounts (see section 3.1), whereas the solubility of other natural iron oxides, such as FeOOH, can even be higher (Zhu et al. 1992). In particular, the iron-induced Cl production may become important concerning aerosol particles with a large fraction of (soluble) iron (e.g. combustion products, volcanic aerosol). For instance, a notable amount of iron-containing aerosol particles and HCl (and other acidic gases) are present in volcanic plumes (Delmelle et al. 2007) and a significant contribution to the observed Cl activation (Gliß et al. 2015) is thinkable.

The iron solubility (and thus the photochemical activity) is a complex function of surface area to volume ratio (Baker and Croot 2010), acid and cloud processing depending on the atmospheric residence time (Zhu et al. 1992; Zhuang et al. 1992; Shi et al. 2009) and the buffer ability. The latter is based on carbonate minerals (e.g. $CaCO_3$ and $MgCO_3$) and thus limits the dissolution of iron into the aqueous aerosol phase (Meskhidze 2005). Ito and Feng (2010) modelled that only a small fraction of iron dissolves in the coarse-mode dust particles (<0.2 %), whereas a significant fraction dissolves in the fine-mode dust particles (1–2 %) above the North Pacific Ocean. In particular, the submicron particles can become very acidic by reaction with HCl or sulfuric acid (Sullivan et al. 2007a, b), and laboratory studies support that the acid processing is the dominant mechanism for iron dissolution in mineral dust during transport (Shi et al. 2012). Potential sources of acidity are trace-gas pollutants (e.g. SO_2, HNO_3, N_2O_5 or HCl). On average, mineral dust particles contain ~3.5 % of iron (Duce and Tindale 1991). The HCl uptake on mineral dust is mainly ascribed to the reaction with $CaCO_{3(s)}$ to form $CaCl_{2(aq)}$ (Tobo et al. 2009). Therefore, HCl can play an important role in forming a deliquescent layer on the particle surface, as Ca-rich dust particles can be converted to aqueous droplets (Tobo et al. 2010). In our study, we found direct evidence that HCl is also taken up by Fe_2O_3 and thus may initiate a catalytic Cl activation cycle in natural environments. The activation may be strengthened in the morning hours after an HCl enrichment in the aerosol during the nighttime. A rough estimate of the uptake coefficient γ (according to Kolb et al. (2010)), based on the calculation of the first order rate constant of the heterogeneous HCl reaction from the measured Cl production rates, leads to a γ between 10^{-4} and 10^{-5}, as compared to $\gamma = 0.14$ for HCl on $CaCO_3$ (Santschi and Rossi 2006).

In general, iron oxides originating from combustion contain a much higher fraction of soluble iron than natural mineral dust (Sedwick et al. 2007; Sholkovitz et al. 2012). Main reasons are the fine mode of the combustion aerosol particles, the missing buffer ability and the presence of acidic gases in combustion plumes. Recently, Wang et al. (2015) estimated a mean combustion source of 5.3 Tg yr^{-1} total Fe from 1960 to 2007 with particle sizes of >10 μm (72 %), 1–10 μm (27 %) and <1 μm (1 %) but an increasing fraction of particles <1 μm since 2000. Fine-grained aerosol particles, produced by combustion, contain 77–81 % soluble iron (Schroth et al. 2009). As a consequence, combustion iron represents typically less than 5 % of total iron deposited over much open ocean regions but can reach fractions up to 20 % close to the continent (Luo et al. 2008). To interpret our results in a larger context, the explored mechanism could be integrated in halogen activation models for tropospheric aerosol particles and clouds (e.g. Herrmann et al. 2003; Tilgner et al. 2013).

5 Conclusions

This study demonstrates the gaseous, iron-catalyzed formation of Cl by uptake of HCl on pure iron-oxide aerosol and iron-oxide dispersed ion in sea-salt aerosol in dependence on the pH. When Fe_2O_3 (Sicotrans Orange, L2515D, BASF) was embedded in an untreated sea-salt matrix, neither a significant amount of dissolved iron nor a significant gaseous Cl production was observed. Adjusting the pH below 3 led to a detectable fraction of dissolved iron that causes significant gaseous Cl productions of $(1.6-1.7)\times10^{21}$ Cl atoms cm^{-2} h^{-1} (pH 2.6), $(5.6-6.6)\times10^{21}$ Cl atoms cm^{-2} h^{-1} (pH 2.2) and $(7.0-9.3)\times10^{21}$ Cl atoms cm^{-2} h^{-1} (pH 1.9). An alternative acceleration of the iron-oxide dissolution by the freezing process (without pH adjustment) could not be observed within the detection limits of our system.

Furthermore, we found evidence for the direct uptake of gaseous HCl on pure iron-oxide aerosol particles and a thereby induced iron-catalyzed production of Cl in the gas phase that can be distinguished significantly from the heterogeneous and homogeneous background production processes of Cl. The various amounts of injected HCl resulted in HCl to Cl conversion rates of 2–5 % at corrected total Cl productions (Q_{eff}) from ~0.8×10^{21} Cl atoms cm^{-2} h^{-1} (at ~41 ppb HCl) to $(41-49)\times10^{21}$ Cl atoms cm^{-2} h^{-1} (at ~345 ppb HCl), whereas the conversion depends on RH and the subsequent uncertainty in the HCl concentrations due to the adsorption effects on the chamber wall and injection losses.

Our findings are of great interest for the processing of iron-containing aerosol in the atmosphere and particularly may become important for the increasing amount of highly soluble combustion aerosol particles in marine environments.

References

Al-Abadleh, H.A.: Review of the bulk and surface chemistry of iron in atmospherically relevant systems containing humic-like substances. RSC Adv. (2015). doi:10.1039/C5RA03132J

Atkinson, R., Baulch, D.L., Cox, R.A., Crowley, J.N., Hampson, R.F., Hynes, R.G., Jenkin, M.E., Rossi, M.J., Troe, J.: Evaluated kinetic and photochemical data for atmospheric chemistry: volume III – Gas phase reactions of inorganic halogens. Atmos. Chem. Phys. (2007). doi:10.5194/acp-7-981-2007

Baker, A.R., Croot, P.L.: Atmospheric and marine controls on aerosol iron solubility in seawater. Mar. Chem. (2010). doi:10.1016/j.marchem.2008.09.003

Baker, A.R., Jickells, T.D., Witt, M., Linge, K.L.: Trends in the solubility of iron, aluminium, manganese and phosphorus in aerosol collected over the Atlantic Ocean. Mar. Chem. (2006). doi:10.1016/j.marchem.2005.06.004

Balzer, N.: Kinetische Untersuchungen der Halogen-Aktivierung einer simulierten Salzpfanne in einer Smogkammer, PhD thesis. University of Bayreuth, Germany (2012). https://epub.uni-bayreuth.de/162/

Bartolomei, V., Gomez Alvarez, E., Wittmer, J., Tlili, S., Strekowski, R., Temime-Roussel, B., Quivet, E., Wortham, H., Zetzsch, C., Kleffmann, J., Gligorovski, S.: Combustion processes as a source of high levels of indoor hydroxyl radicals through the photolysis of nitrous acid. Environ. Sci. Technol. (2015). doi:10.1021/acs.est.5b01905

Behnke, W., Zetzsch, C.: The generation of radicals on aerosol surfaces. Air Poll. Res. Rep. **17**, 119–124 (1988)

Behnke, W., Zetzsch, C.: Heterogeneous production of Cl atoms under simulated tropospheric conditions in a smog chamber. In: Restelli, G., Angeletti, G. (eds.) Physico-Chemical Behaviour of Atmospheric Pollutants, pp. 277–282. Springer, Dordrecht (1990)

Behnke, W., Holländer, W., Koch, W., Nolting, F., Zetzsch, C.: A smog chamber for studies of the photochemical degradation of chemicals in the presence of aerosols. Atmos. Environ. (1988). doi:10.1016/0004-6981(88)90341-1

Bleicher, S., Buxmann, J.C., Sander, R., Riedel, T.P., Thornton, J.A., Platt, U., Zetzsch, C.: The influence of nitrogen oxides on the activation of bromide and chloride in salt aerosol. Atmos. Chem. Phys. Discuss. (2014). doi:10.5194/acpd-14-10135-2014

Buxmann, J., Balzer, N., Bleicher, S., Platt, U., Zetzsch, C.: Observations of bromine explosions in smog chamber experiments above a model salt pan. Int. J. Chem. Kinet. (2012). doi:10.1002/kin.20714

Buxmann, J., Bleicher, S., Platt, U., von Glasow, R., Sommariva, R., Held, A., Zetzsch, C., Ofner, J.: Consumption of reactive halogen species from sea-salt aerosol by secondary organic aerosol: slowing down bromine explosion. Environ. Chem. (2015). doi:10.1071/EN14226

Byrne, R.H., Kester, D.R.: Solubility of hydrous ferric oxide and iron speciation in seawater. Mar. Chem. (1976). doi:10.1016/0304-4203(76)90012-8

Cwiertny, D.M., Young, M.A., Grassian, V.H.: Chemistry and photochemistry of mineral dust aerosol. Annu. Rev. Phys. Chem. (2008). doi:10.1146/annurev.physchem.59.032607.093630

Delmelle, P., Lambert, M., Dufrêne, Y., Gerin, P., Óskarsson, N.: Gas/aerosol–ash interaction in volcanic plumes: new insights from surface analyses of fine ash particles. Earth Planet. Sci. Lett. (2007). doi:10.1016/j.epsl.2007.04.052

Duce, R.A., Tindale, N.W.: Atmospheric transport of iron and its deposition in the ocean. Limnol. Oceangr. (1991). doi:10.4319/lo.1991.36.8.1715

Duggen, S., Croot, P., Schacht, U., Hoffmann, L.: Subduction zone volcanic ash can fertilize the surface ocean and stimulate phytoplankton growth: evidence from biogeochemical experiments and satellite data. Geophys. Res. Lett. (2007). doi:10.1029/2006GL027522

Erickson, D.J., Seuzaret, C., Keene, W.C., Gong, S.L.: A general circulation model based calculation of HCl and $ClNO_2$ production from sea salt dechlorination: reactive chlorine emissions inventory. J. Geophys. Res. (1999). doi:10.1029/98JD01384

Gliß, J., Bobrowski, N., Vogel, L., Pöhler, D., Platt, U.: OClO and BrO observations in the volcanic plume of Mt. Etna – implications on the chemistry of chlorine and bromine species in volcanic plumes. Atmos. Chem. Phys. (2015). doi:10.5194/acp-15-5659-2015

Graedel, T.E., Keene, W.C.: The budget and cycle of earth's natural chlorine. Pure Appl. Chem. (1996). doi:10.1351/pac199668091689

Herrmann, H., Majdik, Z., Ervens, B., Weise, D.: Halogen production from aqueous tropospheric particles. Chemosphere (2003). doi:10.1016/S0045-6535(03)00202-9

Ito, A., Feng, Y.: Role of dust alkalinity in acid mobilization of iron. Atmos. Chem. Phys. (2010). doi:10.5194/acp-10-9237-2010

Jeong, D., Kim, K., Choi, W.: Accelerated dissolution of iron oxides in ice. Atmos. Chem. Phys. (2012). doi:10.5194/acp-12-11125-2012

Jickells, T.D., Spokes, L.J.: Atmospheric iron inputs to the oceans. IUPAC Ser. Analytical Phys. Chem. Environ. Syst. **7**, 85–122 (2001)

Keene, W.C., Savoie, D.L.: The pH of deliquesced sea-salt aerosol in polluted marine air. Geophys. Res. Lett. (1998). doi:10.1029/98GL01591

Keene, W.C., Sander, R., Pszenny, A.A., Vogt, R., Crutzen, P.J., Galloway, J.N.: Aerosol pH in the marine boundary layer. J. Aerosol Sci. (1998). doi:10.1016/S0021-8502(97)10011-8

Keene, W.C., Khalil, M., Aslam, K., Erickson, D.J., McCulloch, A., Graedel, T.E., Lobert, J.M., Aucott, M.L., Gong, S.L., Harper, D.B., Kleiman, G., Midgley, P., Moore, R.M., Seuzaret, C., Sturges, W.T., Benkovitz, C.M., Koropalov, V., Barrie, L.A., Li, Y.F.: Composite global emissions of reactive chlorine from anthropogenic and natural sources: reactive chlorine emissions inventory. J. Geophys. Res. (1999). doi:10.1029/1998JD100084

Kester, D.R., Duedall, I.W., Connors, D.N., Pytkowicz, R.M.: Preparation of artificial seawater. Limnol. Oceangr. (1967). doi:10.4319/lo.1967.12.1.0176

Kiwi, J., Lopez, A., Nadtochenko, V.: Mechanism and kinetics of the OH-radical intervention during Fenton oxidation in the presence of a significant amount of radical scavenger (Cl^-). Environ. Sci. Technol. (2000). doi:10.1021/es991406i

Knipping, E.M., Lakin, M.J., Foster, K.L., Jungwirth, P., Tobias, D.J., Gerber, R.B., Dabdub, D., Finlayson-Pitts, B.J.: Experiments and simulations of ion-enhanced interfacial chemistry on aqueous NaCl aerosols. Science (2000). doi:10.1126/science.288.5464.301

Kolb, C.E., Cox, R.A., Abbatt, J.P.D., Ammann, M., Davis, E.J., Donaldson, D.J., Garrett, B.C., George, C., Griffiths, P.T., Hanson, D.R., Kulmala, M., McFiggans, G., Pöschl, U., Riipinen, I., Rossi, M.J., Rudich, Y., Wagner, P.E., Winkler, P.M., Worsnop, D.R., O' Dowd, C.D.: An overview of current issues in the uptake of atmospheric trace gases by aerosols and clouds. Atmos. Chem. Phys. (2010). doi:10.5194/acp-10-10561-2010

Kuma, K., Nishioka, J.U., Matsunaga, K.: Controls on iron(III) hydroxide solubility in seawater: the influence of pH and natural organic chelators. Limnol. Oceangr. (1996). doi:10.4319/lo.1996.41.3.0396

Lim, M., Chiang, K., Amal, R.: Photochemical synthesis of chlorine gas from iron(III) and chloride solution. J. Photochem. Photobiol., A (2006). doi:10.1016/j.jphotochem.2006.03.005

Liu, X., Millero, F.J.: The solubility of iron in seawater. Mar. Chem. (2002). doi:10.1016/S0304-4203(01)00074-3

Luo, C., Mahowald, N., Bond, T., Chuang, P.Y., Artaxo, P., Siefert, R., Chen, Y., Schauer, J.: Combustion iron distribution and deposition. Glob Biogeochem. Cycles (2008). doi:10.1029/2007GB002964

Machulek, A., Vautier-Giongo, C., Moraes, J.E.F., Nascimento, C.A.O., Quina, F.H.: Laser flash photolysis study of the photocatalytic step of the photo-Fenton reaction in saline solution. J. Photochem. Photobiol. (2006). doi:10.1562/2005-05-28-RA-548

Machulek, A., Moraes, J.E.F., Vautier-Giongo, C., Silverio, C.A., Friedrich, L.C., Nascimento, C.A.O., Gonzalez, M.C., Quina, F.H.: Abatement of the inhibitory effect of chloride anions on the photo-Fenton process. Environ. Sci. Technol. (2007). doi:10.1021/es071884q

Mahowald, N.M., Engelstaedter, S., Luo, C., Sealy, A., Artaxo, P., Benitez-Nelson, C., Bonnet, S., Chen, Y., Chuang, P.Y., Cohen, D.D., Dulac, F., Herut, B., Johansen, A.M., Kubilay, N., Losno, R., Maenhaut, W., Paytan, A., Prospero, J.M., Shank, L.M., Siefert, R.L.: Atmospheric iron deposition: global distribution, variability, and human perturbations. Ann. Rev. Mar. Sci. (2009). doi:10.1146/annurev.marine.010908.163727

Meskhidze, N.: Dust and pollution: a recipe for enhanced ocean fertilization? J. Geophys. Res. (2005). doi:10.1029/2004JD005082

Miller, W.L., King, D., Lin, J., Kester, D.R.: Photochemical redox cycling of iron in coastal seawater. Mar. Chem. (1995). doi:10.1016/0304-4203(95)00027-O

Nadtochenko, V.A., Kiwi, J.: Photolysis of $FeOH^{2+}$ and $FeCl^{2+}$ in aqueous solution. Photodissociation kinetics and quantum yields. Inorg. Chem. (1998). doi:10.1021/ic9804723

Pignatello, J.J., Liu, D., Huston, P.: Evidence for an additional oxidant in the photoassisted Fenton reaction. Environ. Sci. Technol. (1999). doi:10.1021/es980969b

Prescher, C., McCammon, C., Dubrovinsky, L., Moss, A.: A program for analyzing energy-domain Mössbauer spectra from conventional and synchrotron sources. J. Appl. Crystallogr. (2012). doi:10.1107/S0021889812004979

Rossi, M.J.: Heterogeneous reactions on salts. Chem. Rev. **103**, 4823–4882 (2003)

Rubasinghege, G., Lentz, R.W., Scherer, M.M., Grassian, V.H.: Simulated atmospheric processing of iron oxyhydroxide minerals at low pH: roles of particle size and acid anion in iron dissolution. Proc. Natl. Acad. Sci. U. S. A. (2010). doi:10.1073/pnas.0910809107

Santschi, C., Rossi, M.J.: Uptake of CO_2, SO_2, HNO_3 and HCl on calcite ($CaCO_3$) at 300 K: mechanism and the role of adsorbed water. J. Phys. Chem. A (2006). doi:10.1021/jp056312b

Schroth, A.W., Crusius, J., Sholkovitz, E.R., Bostick, B.C.: Iron solubility driven by speciation in dust sources to the ocean. Nat. Geosci. (2009). doi:10.1038/ngeo501

Sedwick, P.N., Sholkovitz, E.R., Church, T.M.: Impact of anthropogenic combustion emissions on the fractional solubility of aerosol iron: evidence from the Sargasso Sea. Geochem. Geophys. Geosyst. (2007). doi:10.1029/2007GC001586

Shi, Z., Krom, M.D., Bonneville, S., Baker, A.R., Jickells, T.D., Benning, L.G.: Formation of iron nanoparticles and increase in iron reactivity in mineral dust during simulated cloud processing. Environ. Sci. Technol. (2009). doi:10.1021/es901294g

Shi, Z., Krom, M.D., Jickells, T.D., Bonneville, S., Carslaw, K.S., Mihalopoulos, N., Baker, A.R., Benning, L.G.: Impacts on iron solubility in the mineral dust by processes in the source region and the atmosphere: a review. Aeolian Res. (2012). doi:10.1016/j.aeolia.2012.03.001

Sholkovitz, E.R., Sedwick, P.N., Church, T.M., Baker, A.R., Powell, C.F.: Fractional solubility of aerosol iron: synthesis of a global-scale data set. Geochim. Cosmochim. Ac. (2012). doi:10.1016/j.gca.2012.04.022

Siefert, R.L., Johansen, A.M., Hoffmann, M.R., Pehkonen, S.O.: Measurements of trace metal (Fe, Cu, Mn, Cr) oxidation states in fog and stratus clouds. J. Air Waste Manag. Assoc. (1998). doi:10.1080/10473289.1998.10463659

Sullivan, R.C., Guazzotti, S.A., Sodeman, D.A., Prather, K.A.: Direct observations of the atmospheric processing of Asian mineral dust. Atmos. Chem. Phys. (2007a). doi:10.5194/acp-7-1213-2007

Sullivan, R.C., Guazzotti, S.A., Sodeman, D.A., Tang, Y., Carmichael, G.R., Prather, K.A.: Mineral dust is a sink for chlorine in the marine boundary layer. Atmos. Environ. (2007b). doi:10.1016/j.atmosenv.2007.05.047

Supeno, Supeno, P.: Sonochemical formation of nitrate and nitrite in water. Ultrason. Sonochem. (2000). doi:10.1016/S1350-4177(99)00043-7

Svensson, R., Ljungström, E., Lindqvist, O.: Kinetics of the reaction between nitrogen dioxide and water vapour. Atmos. Environ. (1987). doi:10.1016/0004-6981(87)90315-5

Tilgner, A., Bräuer, P., Wolke, R., Herrmann, H.: Modelling multiphase chemistry in deliquescent aerosols and clouds using CAPRAM3.0i. J. Atmos. Chem. (2013). doi:10.1007/s10874-013-9267-4

Tobo, Y., Zhang, D., Nakata, N., Yamada, M., Ogata, H., Hara, K., Iwasaka, Y.: Hygroscopic mineral dust particles as influenced by chlorine chemistry in the marine atmosphere. Geophys. Res. Lett. (2009). doi:10.1029/2008GL036883

Tobo, Y., Zhang, D., Matsuki, A., Iwasaka, Y.: Asian dust particles converted into aqueous droplets under remote marine atmospheric conditions. Proc. Natl. Acad. Sci. U. S. A. (2010). doi:10.1073/pnas.1008235107

Vogt, R., Crutzen, P.J., Sander, R.: A mechanism for halogen release from sea-salt aerosol in the remote marine boundary layer. Nature (1996). doi:10.1038/383327a0

Wahner, A., Mentel, T.F., Sohn, M.: Gas-phase reaction of N_2O_5 with water vapor: Importance of heterogeneous hydrolysis of N_2O_5 and surface desorption of HNO_3 in a large Teflon chamber. Geophys. Res. Lett. (1998). doi:10.1029/98GL51596

Wang, W.-N., Purwanto, A., Lenggoro, I.W., Okuyama, K., Chang, H., Jang, H.D.: Investigation on the correlations between droplet and particle size distribution in ultrasonic spray pyrolysis. Ind. Eng. Chem. Res. (2008). doi:10.1021/ie070821d

Wang, R., Balkanski, Y., Boucher, O., Bopp, L., Chappell, A., Ciais, P., Hauglustaine, D., Peñuelas, J., Tao, S.: Sources, transport and deposition of iron in the global atmosphere. Atmos. Chem. Phys. (2015). doi:10.5194/acp-15-6247-2015

Wittmer, J., Bleicher, S., Zetzsch, C.: Iron(III)-induced activation of chloride and bromide from modeled saltpans. J. Phys. Chem. A (2015a). doi:10.1021/jp508006s

Wittmer, J., Bleicher, S., Ofner, J., Zetzsch, C.: Iron(III)-induced activation of chloride from artificial sea salt aerosol. Environ. Chem. (2015b). doi:10.1071/EN14279

Zetzsch, C., Behnke, W.: Heterogeneous reactions of chlorine compounds. In: Niki, H., Becker, K.H. (eds.) The Tropospheric Chemistry of Ozone in the Polar Regions, pp. 291–306. Springer, Berlin Heidelberg (1993)

Zetzsch, C.: Simulation of atmospheric photochemistry in the presence of solid airborne aerosols. In: Dechema-Monographien, vol 104. pp 187–213. Verlag Chemie, Weinheim, Germany (1987)

Zhang, D., Iwasaka, Y.: Chlorine deposition on dust particles in marine atmosphere. Geophys. Res. Lett. (2001). doi:10.1029/2001GL013333

Zhu, X., Prospero, J.M., Millero, F.J., Savoie, D.L., Brass, G.W.: The solubility of ferric ion in marine mineral aerosol solutions at ambient relative humidities. Mar. Chem. (1992). doi:10.1016/0304-4203(92)90069-M

Zhu, X., Prospero, J.M., Savoie, D.L., Millero, F.J., Zika, R.G., Saltzman, E.S.: Photoreduction of iron(III) in marine mineral aerosol solutions. J. Geophys. Res. (1993). doi:10.1029/93JD00202

Zhuang, G., Yi, Z., Duce, R.A., Brown, P.R.: Chemistry of iron in marine aerosols. Glob. Biogeochem. Cycles (1992). doi:10.1029/92GB00756